한국소음진동공학회 2003년도 추계학술대회논문집, pp. 819~823.

Dynamic Stability Regions for Arches

Kwang Kyou Park* · Byoung Koo Lee** · Sang Jin Oh***
Kyu Moon Choi**** and ○Tae Eun Lee*****

Key Words : Shallow parabolic arch, Dynamic critical load, Dynamic stability region, Point step load.

ABSTRACT

The differential equations governing the shape of displacement for the shallow parabolic arch subjected to multiple dynamic point step loads were derived and solved numerically. The Runge-Kutta method was used to perform the time integrations. Hinged-hinged end constraint was considered. Based on the Budiansky-Roth criterion, the dynamic critical point step loads were calculated and the dynamic stability regions for such loads were determined by using the data of critical loads obtained in this study.

1. Introduction

The dynamic behavior of the arch is very important in the fields of structural engineering References[1-6] and their citations included the governing equations and significant historical literatur on the dynamic stability of arches. Budiansky and Roth[1] reported on the axisymmetric dynamic buckling of clamped spherical shells. Lock[2] studied on the snapping of a shallow sinusoidal arch unde the step pressure load. DaDDepo and Schmidt[3] investigated the stability of two-hinged circular arches Lo and Masur[4] reported the dynamic stability boundaries for the sinusoidal arch with pulse loads.

The main purpose of the present paper is to obtain the dynamic stability regions for the shallow parabolic hinged arches. In the numerical examples, the dynamic critical point step loads and the dynamic stability regions for the multiple such loads are reported.

* Member, Professor, Daejeon University
E-mail: kkpark@dju.ac.kr Tel: (042)280-2522
** Member, Professor, Wonkwang University
*** Member, Professor, Provincial College of Damyang
**** Backdoo Plant Co., Ltd.
***** Member, Graduate Student, Wonkwang University

2. Mathematical Model

Figure 1 shows the two-hinged shallow paraboli arch whose span length and rise are L and H, respectively. The dashed line is the netural axis o undeformed arch expressed as $Y_0(X)$. The solid curve is the middle surface of deformed arch due to the multiple dynamic point step loads $P_1(X_1, T)$, $P_2(X_2, T), \cdots, P_M(X_M, T)$, that is depicted as $Y(X, T)$. Here X and Y_0, Y are the rectangular co-ordinate and T is time.

It is assumed that the Bernoulli-Euler beam theory[7] governs the relationship between load and displacement of element of arch subjected to the loads, stress resultants and inertia forces. Then the partial differential equations of the arch element are

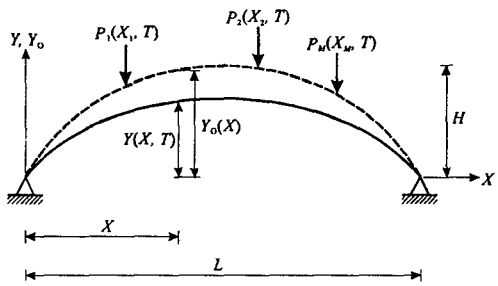

Fig. 1 Shallow parabolic hinged-hinged arch subjected to multiple dynamic point step loads.

$$EI[\,Y(X,T)-Y_0(X)]_{,XXXX}+NY(X,T)_{,XX}+\sum_{i=1}^{M}P_i(X_i,T)+\rho Y(X,Y)_{,TT}=0 \quad (1)$$

$$N=(EA/2L)\int_0^L[\,Y_0{}^2(X)_{,XX}-Y^2(X,T)_{,X}]dX \quad (2)$$

where the subscripts X and T are the operators $\partial/\partial X$ and $\partial/\partial T$, respectively. The EI and EA are the flexural and axial rigidities, respectively. And the ρ is the mass per unit length of X-axis which is assumed to be constant in the shallow arches[6]. In Eq. (1), N is the horizontal thrust which can be calculated by Eq. (2) and is not varied along the X-axis.

Here the following displacement function is introduced as follows.

$$W(X,T)=Y_0(X)-Y(X,T) \quad (3)$$

To facilitate the numerical studies and to obtain the most general results for this class of problems, th following non-dimensional system parameters are cast.

$$x=X/L \quad (4.1)$$

$$y(x,t)=Y(X,T)/(2\sqrt{I/A}) \quad (4.2)$$

$$y_o(x)=Y_o(X)/(2\sqrt{I/A}) \quad (4.3)$$

$$h=H/(2\sqrt{I/A}) \quad (4.4)$$

$$t=(T/L^2)\sqrt{EI/\rho} \quad (4.5)$$

$$p_i(x,t)=P_i(X_i,T)L^3/(2EI\pi^4\sqrt{I/A}),\quad i=1,2,\cdots,M \quad (4.6)$$

When Eq. (3) is substituted into Eqs. (1) and (2), and Eqs. (4.1)-(4.6) are used, the non-dimensional forms of Eqs. (1) and (2) become

$$w(x,t)_{,tt}+w(x,t)_{,xxxx}+nw(x,t)_{,xx}-ny_o(x)_{,xx}=\pi^4\sum_{i=1}^{M}p(x_i,t) \quad (5)$$

$$n=2\int_0^1[2w(x,t)_{,x}y_o(x)_{,x}-w^2(x,t)_{,xx}]dx \quad (6)$$

in which $w(x,t)$ is the non-dimensional form of Eq (3) expressed as

$$w(x,t)=y_o(x)-y(x,t) \quad (7)$$

The boundary conditions for hinged ends are

$$w(0,t)=0,\quad w(0,t)_{,xx}=0 \quad (8.1,\ 8.2)$$

$$w(1,t)=0,\quad w(1,t)_{,xx}=0 \quad (8.3,\ 8.4)$$

3. Shape of Arch and Displacement Function

In this study. the shape of shallow arch and the displacement function of Eq. (7) are selected as parabolic and sinusoidal functions, respectively. First the shape of the parabolic arch $Y_0(X)$ in Fig. 1 can be defined as $Y_0(X)=4H(X^2-2X)/L^2$ and its non-dimensional form obtained by Eqs. (4.3) and (4.4) is

$$y_0(x)=4hx(1-x),\quad 0\le x\le 1 \quad (9)$$

Second, the displacement function of Eq. (7) is given in the form of

$$w(x,t)=y_0(x)-y(x,t)=\sum_{k=1}^{m}a_k(t)\sin(k\pi x),\quad 0\le x\le 1 \quad (10)$$

Here k is the mode number, $a_k(t)$ is the amplitude of kth mode, $\sin(k\pi x)$ is the shape function of k th mode and m is the total mode number considered. It is noted that the displacement function of Eq. (10) satisfies Eqs. (8.1)-(8.4) for the boundary conditions of hinged arches.

Substituting the related partial derivaties obtained by Eqs. (9) and (10) into Eqs. (5) and (6), and integrating from $x=0$ to $x=1$ gives the following Eqs. (11) and (12), respectively.

$$\ddot{a}_k+k^4\pi^4a_k-nk^2\pi^2a_k+(16hn/k\pi)\{1-\cos(k\pi)\}=2\pi^4\int_0^1 p(x,t)\sin(k\pi x)dx \quad (11)$$

$$n=(32h/\pi)\sum_{k=1}^{m}k^{-1}a_k\{1-\cos(k\pi)\}-\sum_{k=1}^{m}k^2\pi^2a_k^2 \quad (12)$$

in which the subscript (˙) is the second derivaties with respect to t. When the dynamic load function $p_i(x_i,t)$ in Eq. (5) is given, the non-dimensional displacement function of Eq. (7) and thrust n can be determined by the appropriate numerical methods.

4. Criterion of Dynamic Critical Loads

The dynamic critical load is defined by the load that the response parameter is suddenly increased due to an infinitesimal load increment. The response parameters of the critical loads are as (1) the ratio of mean deflection to mean rise of arch; (2) the deflection at middle span of arch; (3) the snap-through; and (4) the root square after intergrating the square of the deflection.

In this study, the fourth criterion of above response parameters is used, which is proposed by Budinansky and Roth[1]. By the definition of the fourth criterion, the non-dimensional response parameter u(t) is represented as

$$u(t)=[\int_0^1 w^2(x,t)dx]^{1/2} \qquad (13)$$

5. Numerical Examples and Discussion

Based on the above analysis, a general FORTRAN computer program was written to calculate the dynamic critical point step loads. The Runge-Kutta method was used to perform the time integrations of the differential equations Eqs. (5) and (6), which is popularly used for the initial value problems.

For these studies, suitable convergence of solution was obtained under $m=5$ for obtaining the three figure accuracy of solutions as shown in Fig. 2.

The numerical results, given in Fig. 3-6, are summarized as follows, in which all the load parameters and geometries of arches are expressed in non-dimensional forms. Figure 3 shows the relationship between dynamic critical point step load parameter p_{1cr} and its load position parameter x_1 for one point loading with $h=2, 3, 4$. In the range of $0\le x_1\le 0.5$, the p_{1cr} value decreases, and becomes minimum, and then increases as the load position parameter x_1 increases. From this figure, the most weak position parameter x_1 can be determined. For example, the most weak position parameter x_1 for $h=4$ is 0.34.

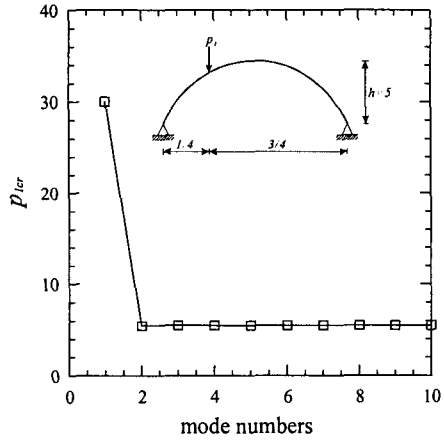

Fig. 2 Convergence of dynamic critical point step loads with increasing number of modes

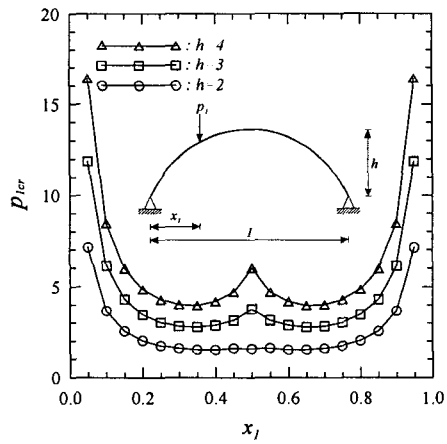

Fig. 3 p_{1cr} versus x_1 curves for one point loading

Figure 4 shows the p_{1cr} versus h curves for on point loading. The p_{1cr} increases as the h increases.

Figure 5 shows the p_{1cr}, p_{2cr} and p_{3cr} versus h curves for three point loads with $x_1=1/4$, $x_2=1/2$ and $x_3=3/4$, respectively. See the load combitation in the legend of this figure.

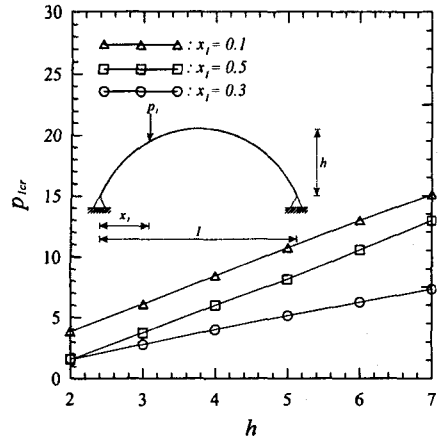

Fig. 4 p_{1cr} versus h curves for one point loading

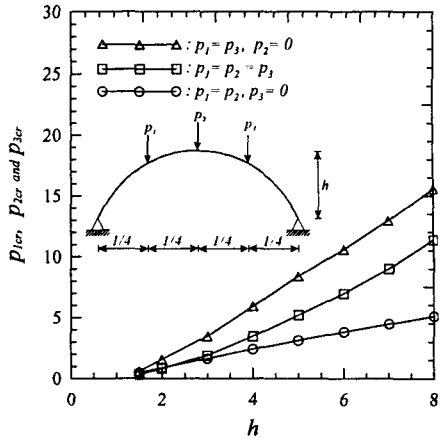

Fig. 5 p_{1cr} , p_{2cr} and p_{3cr} versus h curves for three point loads

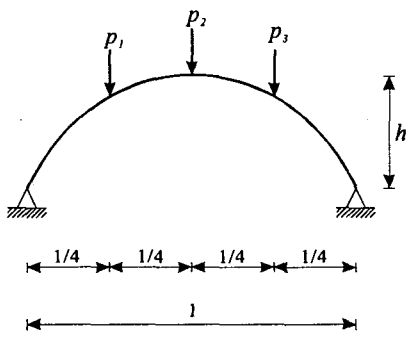

Fig. 6(a) Definition of loads and its positions

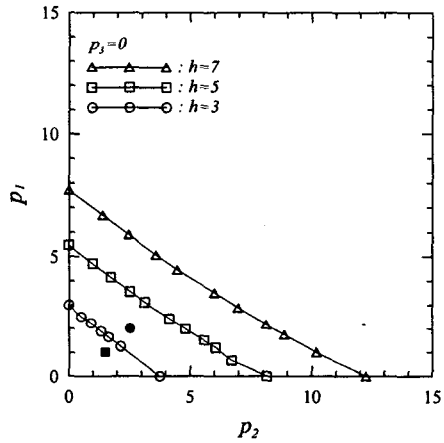

Fig. 6(b) Load case of p_1, p_2 and $p_3 = 0$

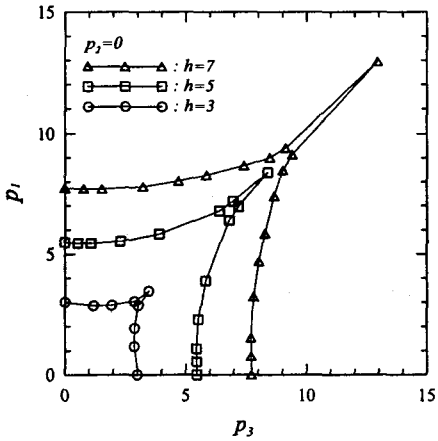

Fig. 6(c) Load case of p_1, $p_2 = 0$ and p_3

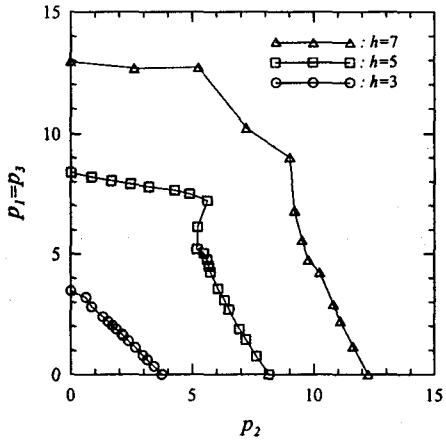

Fig. 6(d) Load case of $p_1 = p_2$ and p_3

Fig. 6 Stability regions for three dynamic point step loads

Figure 6 shows the examples of stability regions of arches subjected to three dynamic point step loads. The load position parameters are defined in Fig. 6(a), and stability regions of three load cases of (p_1, p_2, $p_3=0$), (p_1, $p_2=0$, p_3) and ($p_1=p_3$, p_2) are presented in Fig. 6(b), 6(c) and 6(d), respectively. In these figures, each solid curve is the stability boundary of corresponding case, and the lower part of each stability boundary is the stability region. For example, the load case(h=3) of ($p_1=1$, $p_2=1.5$, $p_3=0$) marked as ■ is safe since this point places in the lower part of stability boundary while that of ($p_1=2$, $p_2=2.5$, $p_3=0$) marked as ● is unsafe since this point places in the upper part in Fig. 6(b).

6. Comcluding Remarks

The differential equations for the multiple dynamic critical point step loads of shallow parabolic hinged arches were formulated and solved numerically. The Runge-Kutta method was used to perform the time integrations and Budiansky-Roth criterion was used to determine the dynamic critical loads. As the numerical results, the dynamic critical point step loads and stability regions are reported in figures. The result obtained in this study can be utilized in the dynamic stability problems of shallow parabolic hinged arches.

References

(1) Budiansky B. and Roth R. S., 1966, "Axisymmetric Dynamic Buckling of Clamped Shallow Spherical Shells," NASA TN D-1510, pp. 597-606.

(2) Lock, M. H., 1966, "Snapping of a Shallow Sinusoidal Arch under a Step Pressure Load," AIAA Journal, Vol. 4, No. 7, pp. 1249-1256.

(3) DaDDepo, D. A. and Schmidt, R., 1974, "Stability of Two-Hinged Circular Arches with Independent Loading Parameters", AIAA Journal, Vol. 12, No. 3, pp. 285-386.

(4) Lo, M. L. C. and Masur, E. F., 1976, "Dynamic Buckling of Shallow Arches", Journal of the Engineering Mechanics Division, ASCE, Vol. 1-2, No. EM5, pp. 901-917.

(5) Donalson, M. T. and Plaut, R. H., 1983, "Dynamic Stability Boundaries for a Sinusoidal Shallow Arch under Pulse Loads", AIAA Journal, Vol. 21. No. 3, pp. 469-471.

(6) Park, K. K., Lee, B. K. and Oh, S. J., 1995, "Dynamic Stability Regions for Parabolic Hinged Arches", Proceeding of SDNVC, pp. 370-375.

(7) Timoshenko, S. P. and Gere, G. M., 1961, Theory of Elastic Stability, McGraw-Hill Book Company, Inc., New York.

(8) Darkov, A. and Kuzetsov, V., Structural Mechanics, Gorden and Brdach.